Published in final edited form as:
Neuroimage. 2010 February 1; 49(3): 2638–2648. doi:10.1016/j.neuroimage.2009.11.008.

When less is more: TPJ and default network deactivation during encoding predicts working memory performance

Alan Anticevic[a,*], **Grega Repovs**[b], **Gordon L. Shulman**[c], and **Deanna M. Barch**[d]

[a]Department of Psychology, Campus Box 1125, Washington University, Saint Louis, MO 63130, USA

[b]Department of Psychology, University of Ljubljana, Slovenia

[c]Department of Neurology, Washington University in St. Louis, Saint Louis, MO 63130, USA

[d]Departments of Psychology, Psychiatry and Radiology, Washington University in St. Louis, Saint Louis, MO 63130, USA

Abstract

Previous work has shown that temporo-parietal junction (TPJ), part of a ventral attention network for stimulus-driven reorienting, deactivates during effortful cognitive engagement, along with the default mode network (DMN). TPJ deactivation has been reported both during working memory (WM) and rapid visual search, ostensibly to prevent reorienting to irrelevant objects. We tested whether the magnitude of this deactivation during WM encoding is predictive of subsequent WM performance. Using slow event-related fMRI and a delayed WM task in which distracter stimuli were presented during the maintenance phase, we found that greater TPJ and DMN deactivation during the encoding phase predicted better WM performance. TPJ and DMN, however, also showed several functional dissociations: (1) TPJ exhibited a different task-evoked pattern than DMN, responding to distracters sharing task-relevant features, but not to other types of distracters; and (2) TPJ showed strong functional connectivity with the DMN at encoding but not during distracter presentation. These results provide further evidence for the functional importance of TPJ suppression and indicate that TPJ and DMN deactivation is especially critical during WM trace formation. In addition, the functional connectivity results suggest that TPJ, while not part of the DMN during the resting state, may flexibly "couple" with this network depending on task demands.

Keywords

TPJ; Working memory; Default network; Functional connectivity

Introduction

Recent studies have defined two broadly distributed but functionally distinct cortical networks involved in allocation of attentional resources: the dorsal and the ventral attention systems (Corbetta et al., 2002, 2008). One key region of the ventral attention system is the right temporo-parietal junction (TPJ), situated at the intersection of the posterior end of the

*Corresponding author. Fax: +1 314 935 8790. aanticev@artsci.wustl.edu (A. Anticevic)..

Appendix A. Supplementary data Supplementary data associated with this article can be found, in the online version, at doi: 10.1016/j.neuroimage.2009.11.008.

superior temporal sulcus and the inferior parietal lobule. Previous work has suggested that TPJ is involved in re-orienting attention to the external environment when behaviorally important stimuli are encountered (Arrington et al., 2000; Corbetta et al., 2000; Downar et al., 2001; Indovina and Macaluso, 2007; Macaluso et al., 2002; Marois et al., 2000; Serences et al., 2005) and that it is maximally responsive to behavioral relevance of stimuli rather than their sensory salience (Indovina and Macaluso, 2007; Kincade et al., 2005). For instance, previous work showed that TPJ is most responsive when an unexpected environmental stimulus is encountered (Downar et al., 2000, 2001, 2002) that matches the features of the current task (Serences et al., 2005). While reorienting to behaviorally important stimuli is critical for an animal's survival, reorienting to irrelevant stimuli may interfere with ongoing task performance. Therefore, during effortful cognitive engagement (e.g., encoding novel information into working memory) it may be advantageous to impose an attentional filter that restricts TPJ activation, protecting the ongoing focus of attention from distraction (Shulman et al., 2003, 2007; Todd et al., 2005).

In line with the idea that TPJ deactivation may be necessary at times, previous work has shown that TPJ is deactivated when cognitive demands are imposed (e.g. WM or difficult perceptual search) and the dorsal attention system is engaged (Shulman et al., 2003; Todd et al., 2005). Shulman and colleagues (2003) showed that TPJ was deactivated in a rapid-visual search paradigm (RSVP) prior to target onset when subjects monitored a stream of letters for a target digit, and that the mean magnitude of deactivation was greater on trials in which the subsequent target was detected than on trials in which it was missed (Shulman et al., 2007). They postulated that the magnitude of TPJ deactivation reflected the degree of “filtering” of irrelevant information, which ensured that attentional resources were directed towards task-relevant candidate targets (Shulman et al., 2007). Related results have been reported in the context of working memory (WM) tasks. Todd and colleagues (2005) demonstrated TPJ suppression during delayed WM and that the magnitude of TPJ suppression increased at higher WM loads, leading them to postulate TPJ suppression as a mechanism for protecting the contents of WM. Because TPJ is responsive to information potentially relevant to the task, it may be particularly important to suppress TPJ activity during WM encoding, when re-orienting might interfere with establishing a novel memory trace. However, previous work on TPJ suppression during WM has not explicitly examined whether the amount of suppression, especially during WM trace formation, is related to behavioral performance, similar to the relationship between suppression and performance that has been observed during rapid visual search (Shulman et al., 2007).

While TPJ is deactivated during certain phases of a task, a well-defined system of regions known as the default mode network (DMN) is deactivated under a broader range of conditions (Buckner et al., 2005; Mazoyer et al., 2001; McKiernan et al., 2003; Raichle et al., 2001; Ralchle and Snyder, 2007; Shulman et al., 1997) and shows highly correlated activity in the resting state (Fox et al., 2005; Greicius et al., 2003). Importantly, unlike TPJ, the DMN is not activated by behaviorally relevant stimuli and functional connectivity studies indicate that TPJ *is not* correlated with the DMN in the resting state (Fox et al., 2005). Because the relationship between TPJ and task-negative/default regions is uncertain, we investigated the degree to which TPJ and DMN regions showed similar properties during WM performance. To our knowledge, only one study has investigated the relationship between the DMN and WM performance (Hampson et al., 2006). However, this study examined across-subject variability in performance as a function of connectivity strength in only *two* default network nodes and did not test whether DMN deactivation is predictive of WM performance within subjects.

Additionally, while TPJ and DMN regions are not functionally coupled in the resting state (Fox et al., 2005), their activity may be correlated during active WM function. One

interesting possibility is that the relationship between TPJ and DMN regions changes as different cognitive demands emerge. Therefore, we explored the relationship between TPJ and the DMN during the encoding and maintenance phases of a WM task.

In summary, the current study addressed three main goals: (1) to examine whether the degree of TPJ deactivation during encoding is predictive of subsequent WM performance; (2) to examine whether there are other regions in which suppression during encoding predicts subsequent WM performance and whether these regions overlap with the DMN; and (3) to characterize the relationship between TPJ and the DMN across different phases of WM.

Materials and methods

Subjects

21 neurologically intact right-handed, healthy adults (8 male and 13 female, mean age=24.95) were recruited from the Washington University community by the Psychology Department subject coordinator. All subjects completed and signed an informed consent approved by the Washington University Institutional Review Board and were paid $25 an hour for their participation.

Materials

Subjects performed a Sternberg-type delayed WM task, which was modeled after the task employed by Dolcos and colleagues (Dolcos et al., 2008; Dolcos and McCarthy, 2006; Sternberg, 1969) (see Fig. 1). The task contained two levels of working memory load (2 or 3 complex geometric shapes) and one of three potential distracter types presented during the maintenance period of the WM task: (1) a task-related geometric shape, which was expected to maximally engage TPJ (Serences et al., 2005); (2) a visually complex neutral image; and (3) an emotional image which was highly distracting and salient, but not task-related. A portion of the trials did not contain distraction (total of 30 blank trials randomized across the experiment, 15 at each WM load), but these trials were not the focus of the current study. Trial types were presented randomly to ensure that subjects had no ability to predict the nature of upcoming distraction and could not resort to a consistent filtering strategy for any of the distracter types. Lastly, we opted for a single instead of multiple distracters to examine whether previously published effects generalize when even less distraction is present.

The memory sets and task-related distracters consisted of complex geometric shapes (Attneave and Arnoult, 1956), which were generated using a Matlab algorithm (Collin and McMullen, 2002). We opted for these stimuli since they were difficult to verbally encode, ensuring maximal modality-specific interference and minimizing subjects' potential use of the articulatory loop for WM maintenance. In other words, we wanted to ensure, as much as possible, that WM trace maintenance is represented in the modality in which distraction was occurring. Also, we wanted to eliminate potential important individual differences in the degree to which subjects can engage verbal maintenance strategies. Memoranda shapes and probes were set to pure black, while task-related distracters were set to a shade of gray to be distinctive from the probes. The emotional and neutral visual distracters were selected from the IAPS stimulus set (Lang et al., 2008) and were equated on luminance, contrast, figure-ground relationships, spatial frequency and color, thus removing previously noted confounds from the stimulus set that may contribute to differences between emotional and neutral stimuli, aside from purely affective properties of the pictures (Bradley et al., 2007; Delplanque et al., 2007; Sabatinelli et al., 2005). All distracters were presented centrally, with a visual angle of 8.5°.

Task design

Subjects performed a total of 180 trials, which were divided into 90 high and 90 low WM load trials. There were 25 task-related, 25 emotional, 25 neutral and 15 distracter-free trials in each load condition. The trial sequence was pseudo-randomized with the constraint that no distracter type could appear in more than 3 consecutive trials (to avoid mood induction via emotional distracters). The memory sets were presented centrally with a visual angle of 15.75 for a duration of 4.4 s followed by a 8.8 second delay. The delay was followed by a 1.1 second presentation of the distracter (if present) and then by a 5.5-s post-distracter delay and a probe presented for 2.2 seconds (see Fig. 1). Each trial was followed by a 13.2-s fixation period to allow the hemodynamic response to return to baseline. Prior to the start of the experiment subjects were given instructions explaining the task as well as a brief (8 trial) practice session to demonstrate various trial combinations. The entire experiment was divided into 12 BOLD scanning sequences, each lasting 9.2 min. During the scanning period stimuli were presented through an LCD projector to a screen located behind the scanner, which the subject could see through an angled mirror located above the eyes.

Data acquisition

All subjects were scanned on a 3T Tim TRIO scanner at Mallinckrodt Institute of Radiology at the Washington University Medical School. Functional images were acquired using an asymmetric spin-echo, echo-planar sequence, which was maximally sensitive to blood oxygenation level-dependent (BOLD) contrast (T2*) (repetition time [TR]=2200 ms, echo time [TE]=27 ms, field of view [FOV]=256 mm, flip=90°, voxel size=4×4×4 mm). 251 whole-brain volumes were acquired during each BOLD run, each volume consisting of 32 oblique axial slices (4×4×4 mm resolution) acquired parallel to the anterior-posterior commissure. Structural images were acquired using a sagittal MP-RAGE 3D T1-weighted sequence (TR=2400 ms, TE=3.16 ms, flip=8°; voxel size=1×1×1 mm).

Data preprocessing

fMRI data preprocessing steps included: (1) compensation for slice-dependent time shifts; (2) removal of first 5 images from each run during which BOLD signal was allowed to reach steady state; (3) elimination of odd/even slice intensity differences due to interpolated acquisition; (4) realignment of data acquired in each subject within and across runs to compensate for rigid body motion (Ojemann et al., 1997); (5) intensity normalization to a whole-brain mode value of 1,000 but without bias or gain field correction; (6) registration of the 3D structural volume (T1) to the atlas representative template based on 12 normal subjects represented in the Talairach coordinate system (Talairach and Tournoux, 1988) using a 12-parameter affine transform and re-sampled to 1 mm cubic representation (Buckner et al., 2004; Ojemann et al., 1997); (7) co-registration of the 3D fMRI volume to the structural image and transformation to atlas space using a single affine 12-parameter transform that included a resampling to a 3-mm cubic representation; and (8) smoothing using a 6 mm full-width at half maximum (FWHM) Gaussian filter.

General fMRI analysis

As a first step a general linear model (GLM) approach was used to estimate magnitudes of task-related activity in each voxel (Worsley and Friston, 1995). We employed an assumed response GLM approach to specifically isolate encoding related activation in addition to other trial components. The model estimated 5 different components of each trial (i.e. encoding, pre-distracter delay, distracter response, post-distracter delay and probe, see Supplemental Fig. S1), obtained by convolving a block function reflecting the neuronal response with a Boynton assumed BOLD response function (Boynton et al., 1996). Distracter response and post-distracter delay were modeled separately for each condition

type, whereas encoding and pre-distracter delay components were not, given that subjects had no advance knowledge of upcoming distracter type. All components were modeled separately for both low and high loads. Of note, given the temporal proximity of the distracter and post-distracter delay components we did not make explicit comparisons between the two components and we specifically used the distracter component for the remainder of analyses. An additional assumed response GLM model was computed that included accuracy as a covariate to enable examination of within-subject trial-by-trial relationship between behavioral performance and brain activity. All subsequent statistical analyses used the beta estimates from the *assumed response* GLM model.

Given the large number of active foci meeting a whole-brain $p<0.05$ correction in the whole-brain analyses all identified maps were partitioned using a peak-splitting algorithm such that peaks were considered as separate if they were more than 10 mm apart (Kerr et al., 2004; Michelon et al., 2003). In addition, to visualize the activation time courses, we used assumption-free models to estimate signal for each condition (i.e. 2 load levels and 3 distracter-type trials, correct versus incorrect) by estimating 15 time points immediately following trial onset (Boynton et al., 1996). Of note, confirming the validity of our modeling approach, all the results using the assumption-free model analysis did not differ from the ones obtained using an assumption-based model. All whole-brain analyses were visualized using Caret 5.5 software (http://brainvis.wustl.edu/wiki/index.php/Caret:Download) and projected on the PALS (population average landmark and surface-based) atlas (Van Essen, 2005).

TPJ ROI identification

To ensure that the TPJ ROI used in the study was defined independently from the current fMRI data, we placed a spherical seed at the center of mass as defined by Shulman et al. (2007) [x=+52, y=−49, z=+26] with a radius of 3 functional voxels. This yielded a 123-voxel TPJ ROI, which we used for all reported analyses, and from which we extracted all reported time courses. We opted for the Shulman and colleagues TPJ ROI given that their data were collected at the Imaging Center of the Mallinckrodt Institute of Radiology at the Washington University Medical School, were preprocessed using similar methods and were aligned to the same atlas space (cf. Shulman et al., 2007). In addition, the same a-priori TPJ ROI was used to conduct seed-based connectivity analyses outlined in later sections.

Default network seeds identification

Given that some of the analyses focused on quantitatively verifying TPJ and DMN activation and connectivity patterns, we employed the same approach as with TPJ ROI to independently identify all DMN seeds as defined by Fox and colleagues (2005). Using center of mass coordinates from Fox and colleagues (2005) we generated spherical seeds with a radius of 3 voxels for each DMN node. This produced a total of 13 spherical 123-voxel ROIs, which were used to investigate TPJ vs. DMN task-evoked signal, ROI-based connectivity computation and verification of functional connectivity differences at different WM phases (outlined bellow).

Functional connectivity preprocessing

Prior to performing functional connectivity (fcMRI) analyses, all BOLD time series were further preprocessed to remove possible sources of spurious correlations. All preprocessing, as well as further fcMRI analyses, were performed using in-house software implemented in Matlab 7.4 and were based on previously published fcMRI techniques (Fox et al., 2005). (1) All images were spatially smoothed using a 6-mm FWHM Gaussian filter (as in the GLM computation above). (2) To remove low frequencies and scanner drift, images were temporally filtered using a high-pass filter with a cutoff frequency of 0.009 Hz. (3) Modeled

after the procedure employed by Fox and colleagues (2005) a set of nuisance regressors was removed from the signal using multiple regression and included: 6 rigid body motion correction parameters, ventricle signal, deep white matter signal and whole-brain signal. Whole-brain and ventricle regions were defined individually for each BOLD run based on its first frame volume using an automated algorithm. Brain edge was identified using a fixed threshold. Ventricle centers were identified by peak intensities within a predefined search volume. Their extent was defined by an iterative algorithm that searched for large changes in intensity using previously identified peaks as seeds. Eyes were excluded based on a predefined mask. As a final step, one layer of boundary voxels was excluded from both whole-brain and ventricle regions to remove any possible remaining overlap. All the nuisance regressors were also expressed as their first temporal derivative to remove their temporally shifted versions. All subsequent fcMRI analyses were based on the residual signal after removal was carried out for the listed nuisance regressors.

Seed-based whole-brain correlation analysis

As described in Introduction, we wanted to investigate the relationship between TPJ and DMN regions at different phases of WM to examine whether this relationship changes as the WM process unfolds. Our first step in addressing this question was to compute and compare whole-brain seed-based correlation maps at the encoding and distracter phases of the WM trial using the TPJ ROI as a seed region (described above). To accomplish this we computed the average BOLD signal value during the encoding (average of time points 3 and 4) and distracter phases (average of time points 8 and 9) at each trial for each voxel in the image. These values were then concatenated into two 4D (brain volume by trial) series representing encoding and distracter phase responses over all the trials. TPJ correlation maps were computed by extracting average values across all the voxels in the TPJ ROI and computing their correlation with each voxel in the brain. Importantly, the described approach (i.e. using isolated time points during each trial and not all the frames in a trial) effectively enabled us to estimate correlations based on trial-to-trial variability independent of task structure and avoiding spurious correlations due to overall task response. Next, encoding and distracter phase fcMRI maps were computed for each subject separately. We estimated group-level statistical significance by converting individual subjects' correlation maps to Fisher *Z* maps and computing one-sample *t*-tests for each voxel, comparing the correlation against zero. Similarly, statistical significance of differences in fcMRI between different phases of the trial was computed by performing a paired *t*-test between encoding and distracter phase Fisher Z values across subjects. All statistical maps were appropriately corrected for multiple comparisons using cluster size Monte Carlo algorithms to ensure that the obtained foci met whole-brain false positive rates of $p<0.05$.

ROI based TPJ-default network analyses

The second step in testing the relationship between TPJ and DMN was to explicitly quantify correlations within DMN ROIs and between TPJ and DMN ROIs at encoding and distracter phase of the trial. This was accomplished by extracting mean signal values for both TPJ and all DMN ROIs in the same manner as described in the previous section. This enabled us to compute correlations between all pairs of ROI during encoding and distracter phases separately for each subject. All the obtained correlations were converted to Fisher *Z* values and then entered into a two way: *trial phase* (encoding vs. distracter phase)×*connection type* (within-DMN connections vs. TPJ-to-DMN connections) repeated measures ANOVA.

Results

Behavioral performance

We examined behavioral performance both for the fMRI sample only (N=21) and by combining the fMRI sample and additional subjects who completed an identical protocol outside of the scanner (N=19) for maximal power. Fig. 2 shows the complete profile of behavioral results. Mean accuracy for the full sample (N=40) was 76.71% for high and 82.65% for low load condition, indicating that the high load was more behaviorally challenging. To confirm this statistically we computed a 2-way ANOVA with 4 levels of *condition type* (task-related, emotional, neutral and distracter-free conditions) and 2 levels of *load* (high and low). We found a significant *main effect of load* [$F(1,39)=103.62$, $p<0.0001$], a significant *main effect of distracter type* [$F(3,117)=3.95$, $p<0.01$] and a *load by distracter type interaction* [$F(3,117)=9.17$, $p<0.0001$]. The source of the interaction can be explained by examining the differential effects of distraction at high versus low load. In the low load: both task-relevant and emotional distracter conditions were more difficult than the neutral and distracter-free conditions. However, in the high load condition, performance did not differ between neutral and emotional distracters, and task-related distracters were less distracting than either emotional or neutral distracters.

Surprisingly, performance in the distracter-free condition under high WM load was lower than in the distracter conditions. This pattern of behavioral results was unexpected and may reflect an artifact of the experimental design. One possibility is that since distracter trials were much more common than no-distracter trials and presentation was randomized, subjects may have been surprised by the probe stimulus on the latter trials, especially under more difficult conditions (where WM traces may be more vulnerable). Additional out-of-scanner data from our laboratory using identical stimuli supports this hypothesis—WM performance on distracter-free trials was considerably better when they were presented in a separate initial block than when mixed with all the distracter trials. Briefly, as shown in Supplemental Fig. S4, when distracter-free trials were blocked rather than mixed with the rest of distracter trials, performance was better for distracter-free conditions at both WM load levels when compared to distracter trials. This suggests that the distracters used in the present study did indeed provide some level of interference compared to a non-interleaved distracter-free condition. Nevertheless, the distracter-free condition in the current fMRI sample still fails to accurately represent trials without distraction and for this reason we omitted the distracter-free trials from further fMRI analyses. Bellow we compare the neural activity for different distracter trials rather than comparing the activity on distracter and distracter-free trials.

Task-evoked TPJ signal

As a first step we sought to replicate previous findings of TPJ suppression during WM (Todd et al., 2005). Figs. 3A–B shows the TPJ ROI and the extracted task-evoked time course averaged across distracter conditions, since our main hypotheses concerned the signal at encoding and participants had no knowledge at that point of the upcoming distracter. TPJ was significantly suppressed during encoding [$t(20)=-3.17$, $p<0.005$, two-tailed] (see Fig. 3B) and this deactivation persisted until distracter presentation (dotted vertical line marked by arrow), replicating previous findings (Todd et al., 2005). However, we failed to observe load-dependent TPJ suppression either during encoding [$t(20)=0.06$, $p=0.95$] or pre-distracter delay phases [$t(20)=0.47$, $p=0.64$], possibly due to the difficulty of our WM task (see Discussion).

Is TPJ deactivation at encoding predictive of WM performance?

Previous studies have shown that TPJ suppression during visual monitoring, prior to target onset, improves subsequent target detection (Shulman et al., 2007) and others have hypothesized that TPJ suppression may aid WM performance (Todd et al., 2005). Here we explicitly tested if TPJ suppression at encoding and at different phases of the WM trial predicts behavioral performance.

We used a GLM in which correct and incorrect trials were modeled separately (see Materials and methods), allowing us to directly examine-within each subject-differences in BOLD signal magnitude at different phases of the WM process as a function of accuracy. The corresponding TPJ time courses from this analysis for correct (green lines) and incorrect (red dotted lines) trials are shown in Fig. 3C. As before, we collapsed across distracter types, given that at encoding participants had no knowledge of the upcoming distraction. We also averaged across load, given that a similar signal pattern was observed at both load levels. The time courses in Fig. 3C indicated that the TPJ signal was markedly suppressed during encoding and a paired *t*-test indicated that this suppression was significantly greater on correct than incorrect trials [$t(13)=-5.52$, $p<0.0001$]. As with the average task-evoked signal, the pattern did not differ across load [$t(13)=0.36$, $p=0.72$]. However, the pre-distracter delay phase component did not show significantly greater suppression on accurate than inaccurate trials [$t(13)=-0.27$, $p=0.79$], a result that did not differ as a function of load [$t(13)=1.29$, $p=0.22$]. Finally there were no differences between correct and incorrect trials for the distracter component, as evident in Fig. 3C [$t(13)=-0.25$, $p=0.8$]. To confirm that the distracter component did not differ as a function of accuracy, load, or distracter type we computed a 3-way ANOVA with *accuracy* (correct, incorrect), *distracter type* (neutral, emotional, task-related) and *load* (high, low) as factors. No term reached significance. Taken together, these results indicate that greater TPJ suppression specifically during encoding was predictive of better WM performance irrespective of WM load.

Are there other brain regions showing a relationship between deactivation during encoding and WM performance?

We examined if the degree of suppression in any brain region other than the TPJ predicted better WM performance. Beta estimates during encoding for correct and incorrect trials, averaged over distracter type, were compared using a whole-brain voxel-level *t*-test, corrected for multiple comparisons ($Z>3$, cluster size=13 voxels). This analysis revealed a set of brain regions showing significantly less activation for correct vs. incorrect trials (Fig. 4A) that closely matched the DMN, including bilateral posterior medial, bilateral frontal medial, bilateral superior frontal and bilateral inferior temporal cortical regions, bilateral angular gyrus, and bilateral hippocampal gyrus. We carried out additional analyses confirming that the deactivated foci fell largely within the DMN as defined by Fox and colleagues (2005) (see Supplemental Results). Next we isolated each ROI using a peak-splitting approach (see Supplemental Results) to confirm that the obtained deactivated foci showed the same time course pattern of greater deactivation during encoding for correct than incorrect trials. Fig. 4B shows the signal in DMN foci for correct and incorrect trials collapsed across all conditions (given no differences at encoding across load or distracter condition), and indicates more deactivation at encoding for correct trials. This pattern is also illustrated in Fig. 4B (black lines) averaged across all isolated peaks. We carried out additional analyses to confirm that this pattern was also present for: (1) foci explicitly overlapping the DMN map as defined by Fox and colleagues (2005); and (2) for spherical ROIs defined explicitly using Fox and colleagues (2005) center of mass coordinates (Supplemental Materials and Supplemental Fig. S2A–C). As with TPJ, none of the brain regions showing less signal at encoding for correct vs. incorrect trials showed a similar result at pre-distracter delay or distracter response phases of the WM trial.

Do default regions deactivated during encoding show the same overall signal pattern as TPJ?

Because TPJ and DMN showed very similar task-evoked activation profiles during encoding, we examined whether they showed similar profiles during the distracter and probe phases. We used spherical DMN ROIs defined in the same way as TPJ (see Materials and methods). Foci were combined into a single binary "region" file comprised of all DMN ROIs as defined by Fox and colleagues (2005) to compute the overall response within the DMN. To determine whether this response differed from the TPJ response during the distracter phase, we computed a 3-way ANOVA with *distracter type* (neutral, emotional, task-related) × *load* (hi, low)× *region* (TPJ, DMN) as factors. The ANOVA results indicated a significant *region*×*distracter type* interaction [$F(2,40) = 7.87$, $p<0.0015$]. The source of the interaction can be seen in Fig. 5, which indicates in line with previous work (Serences et al., 2005) that TPJ was maximally responsive to task-related distracters, whereas the DMN showed similar response magnitudes across the different distracter types. The main effect of *region* and other terms involving the *region* factor were not significant, indicating no differences as a function of load and no difference in the overall distracter response between TPJ and DMN.

In addition, we compared TPJ vs. DMN response at the probe phase. No significant differences were observed between TPJ and DMN, either overall [$F(1,20)=1.51$, $p=0.23$] or as a function of load [$F(1,20)=0.78$, $p=0.38$]. However, this lack of difference between TPJ and DMN at the probe phase appeared to be largely due to the response of one of the DMN ROI (i.e. retrosplenial cortex), which showed a substantially more prominent probe response when compared to other DMN foci (see Supplemental Fig. S2C). Further, the retrosplenial cortex ROI was not deactivated during encoding, unlike the other DMN ROIs. Although this ROI was identified as a part of the DMN in the resting state using a functional connectivity criterion (Fox et al., 2005, 2006) retrosplenial cortex does not appear to deactivate along with the rest of the DMN nodes during active cognitive states (Shulman et al., 1997). When we conducted the above analysis without the retrosplenial DMN ROI, TPJ showed a significantly higher probe response compared to the rest of the DMN [$F(1,20)=7.43$, $p<0.015$]. Since this exclusion was ad-hoc, however, the difference in the probe response between TPJ and DMN must be considered provisional. Overall, these analyses indicate that the task-induced response pattern in the DMN during the distracter phase and possibly the probe phase was different than that found in TPJ.

fcMRI analyses of the relationship between TPJ and the DMN

We further examined the relationship between TPJ and DMN during encoding and distracter phases of the trial using the TPJ ROI as a seed in trial-based fcMRI analyses. We averaged across all trial types and load levels at each WM phase separately to gain maximal power. Fig. 6A shows the pattern of trial-based connectivity between the TPJ seed and the rest of the brain during encoding (average of time points 3 and 4). Importantly, the use of a single time measurement on each trial ensured that changes within the trial in task structure did not contribute to the observed correlation pattern. Regions showing positive correlations with the TPJ seed at encoding included bilateral anterior medial and posterior medial cortex, bilateral superior temporal sulcus, superior frontal cortex and bilateral angular gyrus (Fig. 6A, red-yellow foci). Conversely, regions showing negative correlations included bilateral intraparietal sulcus, bilateral region MT, bilateral insula/frontal operculum, bilateral frontal eye fields and bilateral SMA (Fig. 6A, blue-green foci). Overall, the positive correlation map showed strong similarity to the DMN map reported by Fox and colleagues (2005) (total overlap with Fox et al., 2005 map was calculated and is shown in Supplemental Fig. S3), while the negative correlation map showed strong correspondence to the fronto-parietal task network (Corbetta et al., 2002), as well as other regions in frontal cortex and insula.

Next, we examined whether the pattern of trial-based fcMRI between the TPJ and the DMN changed as the WM process unfolded. We carried out the same trial-based fcMRI analysis during the WM distracter phase (average of time points 8 and 9). Fig. 6B shows that the pattern of TPJ trial-based connectivity during distracter phase demonstrated many similarities to the pattern found during encoding. Nevertheless, functional connectivity during distracter and encoding phases showed significant differences, as indicated by a whole-brain paired *t*-test using individual Fisher *Z* values that compared encoding vs. distracter phase TPJ trial-based connectivity (Fig. 6C). Fig. 6C indicates that the TPJ showed a decrease in trial-based correlation with the DMN foci during the distracter phase as compared to encoding (indicative of "decoupling" between TPJ and DMN during distraction), but an increase in correlations with most regions of the dorsal fronto-parietal task network including other frontal regions and anterior insula. In summary, these results suggest that as the WM process unfolded, TPJ coupling with the DMN decreased, whereas coupling with the dorsal attention system increased.

The same analysis was conducted using a canonical posterior medial cortex (precuneus) DMN ROI, which was identified using the center of mass as defined by Fox and colleagues (2005) and was the same size as TPJ (123 voxels) (see Materials and methods for more details). The trial-based connectivity pattern at encoding for precuneus was quite similar to that found in the TPJ (Fig. 7A). However, unlike TPJ, precuneus remained coupled with the rest of the DMN during the distracter phase (Fig. 7B) and showed marked attenuation of trial-based connectivity changes from encoding to distracter phase (Fig. 7C). These results indicate that "de-coupling" with the DMN during the distracter phase observed in the TPJ was not apparent when examining a canonical DMN seed.

We confirmed the above results from the voxel-based analysis using a ROI-based analysis that allowed us to explicitly compare TPJ vs. DMN connectivity patterns and to use all DMN regions as ROIs, not just the precuneus. Two questions were investigated: (1) Does TPJ connectivity with explicitly defined DMN ROIs "weaken" from the encoding phase to the distracter phase of WM?; (2) Does connectivity within the DMN remain stable throughout the WM process? We employed a ROI-based fcMRI analysis using all 13 DMN nodes explicitly defined based on the Fox and colleagues (2005) center of mass coordinates that were the same size as the TPJ (see Materials and methods). Correlations were computed between all ROI pairs for each subject and then converted to Fisher *Z* values. The connections at encoding and distracter phases were divided into: (1) DMN-to-DMN correlations, reflecting only DMN pairs excluding TPJ and (2) TPJ-to-DMN correlations reflecting all correlations between DMN nodes and TPJ. Results shown in Fig. 8 indicate that DMN-to-DMN correlations remained relatively stable at encoding and distracter phases; however, TPJ-to-DMN 'coupling' weakened from encoding to distracter phase. To confirm this statistically, we computed a 2-way: *trial phase* (encoding vs. distracter phase) ×*connection type* (DMN-to-DMN connections vs. TPJ-to-DMN connections) repeated measures ANOVA with subjects treated as the random factor. The ANOVA results indicated a significant main effect of *phase* [$F(1,20)=16.97$, $p<0.0006$], main effect of *connection type* [$F(1,20)=5.1$, $p<0.04$] and a significant *trial phase*×*connection type* interaction [$F(1,20)=15.75$, $p<0.0008$]. The source of the interaction, as evident in Fig. 8, was stable within-DMN coupling irrespective of trial phase, but markedly weaker TPJ-to-DMN coupling at distracter phase. Taken together, these results indicate that DMN-to-DMN coupling remains stable throughout WM phases, whereas TPJ-to-DMN coupling weakens as the WM process unfolds.

Discussion

The current study extends our understanding of TPJ function by showing that: (1) TPJ suppression at encoding, prior to distracter onset, predicts better WM performance and (2) the relationship between TPJ and DMN regions changes over the course of the WM process. DMN regions show greater suppression for correct vs. incorrect trials during the encoding phase, similar to TPJ, but show different activity patterns than TPJ during later phases of the trial. Similarly, TPJ activity is coupled with DMN activity during the encoding phase, but de-couples with the DMN during the distracter phase, when it shows stronger correlations with nodes of the dorsal attention network including dorsal frontal and parietal regions.

TPJ suppression during encoding

Previous models of TPJ function have proposed that TPJ is activated in conjunction with dorsal fronto-parietal regions when attentional re-allocation is needed (Corbetta et al., 2002). Given this function, TPJ suppression may be needed when focused attention has to be maintained, thus preventing reorienting to irrelevant objects (Shulman et al., 2007). While a version of the filter hypothesis was formulated in the context of perceptual search (Shulman et al., 2003), it has also been shown that TPJ is suppressed during WM function (Todd et al., 2005). Here we showed that more TPJ suppression during encoding was predictive of better WM performance within subjects. The link between TPJ deactivation during encoding and WM performance supports the filter hypothesis and suggests that TPJ deactivation results in more efficient encoding of novel information into WM. One possibility is that TPJ suppression during encoding (along with suppression of other regions) may be necessary to disengage operations (e.g. orienting) that can potentially disrupt optimal WM trace formation. An important direction for future work will be to more completely characterize TPJ response properties during WM trace formation when encoding may be compromised via distraction.

TPJ function and working memory

The current results did not support the hypothesis that TPJ deactivation, either during encoding or at later time points, improves WM function by preventing subsequent TPJ activity to non-target objects. The average TPJ activity to distracters was very similar on correct and incorrect trials. While we cannot draw firm conclusions regarding TPJ activity to non-target objects (see bellow), one possibility is that-while TPJ activation is undesirable during novel WM trace formation-once a strong WM trace is achieved TPJ may be “freed up” to respond to incoming behaviorally relevant information based on top-down signals established during WM encoding (Corbetta et al., 2002, 2008; Desimone and Duncan, 1995; Folk et al., 1992; Miller and Cohen, 2001; Posner et al., 1980; Treue, 2003). “Freeing up” orienting responses during WM maintenance may allow flexible detection and incorporation of additional environmental inputs in parallel with WM maintenance, thus resulting in a more flexible behavioral repertoire. Therefore, TPJ suppression may be critical while WM traces are being formed and are still fragile (as demonstrated by suppression results during encoding), but once the memory trace has been robustly instantiated, elevated TPJ signals may not provide an additional source of interference.

Alternatively, distracters in the current paradigm may not have produced enough interference to warrant filtering via TPJ in the first place. While overall performance during distraction was far from perfect (79.6% correct, N=40), performance in the distraction-free condition was lower (76.8% correct, N=40), stemming from the surprisingly low accuracy in the distraction-free condition under high WM load (68.6% correct, N=40). As noted earlier, while this is likely an artifact of the present experimental design (i.e. mixing distracter and distracter-free trials rather than blocking) it is still critical for future work to demonstrate the

absence of TPJ deactivation in response to distracters even when such distraction results in worse WM performance when compared to distracter-free trials. Similarly, it will be important for future work to determine whether creating even more interference–such as including multiple distracters–substantially alters present findings, as it may be possible that TPJ responses change substantially when multiple interfering stimuli are present.

In contrast to previous findings, we failed to observe a load-dependent TPJ suppression (Todd et al., 2005). One possible reason may be the strength of the present load manipulation. Our load manipulation consisted of *three vs. two* memoranda items, with a performance cost of 5.5% associated with the higher WM load (ignoring the distracter-free condition). However, the manipulation employed by Todd et al. (2005) consisted of *three vs. one* memoranda item, with a performance cost of 11.34% associated with the higher WM load. This discrepancy in difficulty between WM loads may have produced the difference in load-dependent TPJ suppression. The easier load manipulation in prior work resulted in near ceiling performance (i.e. 94.13% correct), whereas the easier load manipulation in the present study was virtually identical to the harder load manipulation in prior work. In other words, our two-item memoranda set may have produced near-maximal TPJ deactivation such that the higher load added minimal further TPJ suppression resulting in the absence of substantial load effects.

Lastly, some previous work focusing on subsequent memory effects in WM (Pessoa et al., 2002) employed a blocked rather than random presentation of distracters or trials (Sakai et al., 2002). One possibility is that TPJ deactivation does not aid WM performance if the nature of distraction is known a-priori (e.g. when distracter types are blocked) as there may be other brain regions that mediate distracter resistance in such instances (as shown by Sakai et al. 2002). It will be important for future work to further characterize TPJ signals when upcoming distraction is known vs. when it is not.

Default network suppression during encoding

A main finding was that a number of regions closely matching the DMN also showed more suppression for correct vs. incorrect trials during encoding, but not during later stages of WM. As with TPJ, these results suggest that suppressing the DMN during formation of novel memory traces may be critical for optimal WM operation. Considering the proposed functions of the DMN (e.g. daydreaming, thinking about one's future and past, broad internal information evaluation) (Antrobus, 1991; Antrobus et al., 1970; Buckner and Carroll, 2007; Mason et al., 2007; Mazoyer et al., 2001; Raichle et al., 2001; Ralchle and Snyder, 2007) deactivation of the DMN may be critical at times of sustained cognitive engagement with the environment and especially during formation of memory representations. Also, given the putative importance of temporarily “deactivating” the TPJ to achieve attentional filtering, TPJ and DMN regions may become coupled when their temporary disengagement is imperative, thus ensuring robust WM trace formation.

Relationship between TPJ and the default network

TPJ was coupled with DMN regions during encoding of information into WM, although this coupling is not observed in the resting state (Fox et al., 2005; He et al., 2007). Interestingly, this pattern of trial-based connectivity with the DMN changed as the WM process unfolded, with less connectivity during the distracter phase. The opposite pattern of connectivity was observed between the TPJ and components of the dorsal attention system (as well as MFG and other frontal and anterior insula regions) supporting the hypothesis that TPJ signals reflect an “orienting” function separate from the function of the DMN. Thus, TPJ may interact with the dorsal attention system as novel task-relevant information emerges in the external environment and needs to be evaluated in parallel while WM traces are actively

maintained (Corbetta et al., 2008). Consistent with these different functional roles of TPJ and DMN, TPJ showed greater responsiveness than DMN specifically to distracters sharing features with the current task (Serences et al., 2005). In summary, the fcMRI findings suggest that the TPJ may not be functionally static, but instead may dynamically connect with different networks depending on ongoing task demands.

Limitations and future directions

One of the main limitations of this study is the correlational nature of fMRI data and behavior. It will be important for future work to confirm present findings by employing methods that could establish more direct causal links between TPJ function and behavior (e.g. TMS). Furthermore, given the relatively slow time resolution of fMRI it is at present unknown precisely when de-coupling from the DMN nodes may occur. To better understand the precise temporal pattern of TPJ and the DMN interaction the use of other converging non-invasive techniques with more precise timing will be important (e.g. MEG and EEG). One important consideration for future studies of TPJ function, both in the context of attentional processes and other putative TPJ functions (e.g. theory of mind studies), is that TPJ dynamics may be time sensitive both in terms of activation patterns and pattern of connectivity with other brain regions. These dynamics may depend on changing task demands and this consideration becomes particularly important when interpreting TPJ function in the context of experiments using blocked designs, which average activity over possibly diverse processes.

Conclusion

The current study extended our understanding of TPJ function by demonstrating the functional significance of TPJ and DMN suppression when WM traces are still forming. Additionally, we presented evidence that TPJ strongly couples with the DMN during encoding, but dissociates from the DMN both in terms of task-evoked signals and functional connectivity during later WM stages. An important venue for future research will be to better characterize TPJ dynamics during WM trace formation in the presence of distraction as well as the functional importance of changing connectivity between TPJ and other brain regions.

Supplementary Material

Refer to Web version on PubMed Central for supplementary material.

Acknowledgments

We thank T. Braver for helpful comments and analysis suggestions. We also thank M. Fox for allowing us to use previously published data to verify our findings. Supported by NIMH grant MH06603101 (DMB) funded by the National Institute of Mental Health.

References

Antrobus J. Dreaming: cognitive processes during cortical activation ad high afferent thresholds. Psychol. Rev. 1991; 98:96–121. [PubMed: 2006234]

Antrobus JS, Singer JL, Goldstein S, Fortgang M. Mindwandering and cognitive structure. Trans. N. Y. Acad. Sci. 1970; 32:242–252. [PubMed: 5265228]

Arrington CM, Carr TH, Mayer AR, Rao SM. Neural mechanisms of visual attention: object-based selection of a region in space. J. Cogn. Neurosci. 2000; 12:106–117. [PubMed: 11506651]

Attneave F, Arnoult MD. The quantitative study of shape and pattern perception. Psychol. Bull. 1956; 53:452–471. [PubMed: 13370691]

Boynton GM, Engel SA, Glover GH, Heeger DJ. Linear systems analysis of functional magnetic resonance imaging in human V1. J. Neurosci. 1996; 16:4207–4221. [PubMed: 8753882]

Bradley MM, Hamby S, Löw A, Lang PJ. Brain potentials in perception: picture complexity and emotional arousal. Psychophysiology. 2007; 44:364–373. [PubMed: 17433095]

Buckner RL, Carroll DC. Self-projection and the brain. Trends Cogn. Sci. (Regul. Ed.). 2007; 11:49–57. [PubMed: 17188554]

Buckner RL, Head D, Parker J, Fotenos AF, Marcus D, Morris JC, Snyder AZ. A unified approach for morphometric and functional data analysis in young, old, and demented adults using automated atlas-based head size normalization: reliability and validation against manual measurement of total intracranial volume. NeuroImage. 2004; 23:724–738. [PubMed: 15488422]

Buckner RL, Snyder AZ, Shannon BJ, LaRossa G, Sachs R, Fotenos AF, Sheline YI, Klunk WE, Mathis CA, Morris JC, Mintun MA. Molecular, structural, and functional characterization of Alzheimer's disease: evidence for a relationship between default activity, amyloid, and memory. J. Neurosci. 2005; 25:7709–7717. [PubMed: 16120771]

Collin CA, McMullen PA. Using Matlab to generate families of similar Attneave shapes. Behavior Research Methods, Instruments, & Computers: a Journal of the Psychonomic Society, Inc. 2002; 34:55–68.

Corbetta M, Kincade JM, Shulman GL. Neural systems for visual orienting and their relationships to spatial working memory. J. Cogn. Neurosci. 2002; 14:508–523. [PubMed: 11970810]

Corbetta M, Kincade MJ, Ollinger JM, McAvoy MP, Shulman GL. Voluntary orienting is dissociated from target detection in human posterior parietal cortex. Nat. Neurosci. 2000; 3:292–297. [PubMed: 10700263]

Corbetta M, Patel G, Shulman GL. The reorienting system of the human brain: from environment to theory of mind. Neuron. 2008; 58:306–324. [PubMed: 18466742]

Delplanque S, N'diaye K, Scherer K, Grandjean D. Spatial frequencies or emotional effects? A systematic measure of spatial frequencies for IAPS pictures by a discrete wavelet analysis. J. Neurosci. Methods. 2007; 165:144–150. [PubMed: 17629569]

Desimone R, Duncan J. Neural mechanisms of selective visual attention. Annu. Rev. Neurosci. 1995; 18:193–222. [PubMed: 7605061]

Dolcos F, McCarthy G. Brain systems mediating cognitive interference by emotional distraction. J. Neurosci. 2006; 26:2072–2079. [PubMed: 16481440]

Dolcos F, Diaz-Granados P, Wang L, McCarthy G. Opposing influences of emotional and non-emotional distracters upon sustained prefrontal cortex activity during a delayed-response working memory task. Neuropsychologia. 2008; 46:326–335. [PubMed: 17765933]

Downar J, Crawley AP, Mikulis DJ, Davis KD. A multimodal cortical network for the detection of changes in the sensory environment. Nat. Neurosci. 2000; 3:277–283. [PubMed: 10700261]

Downar J, Crawley AP, Mikulis DJ, Davis KD. The effect of task relevance on the cortical response to changes in visual and auditory stimuli: an event-related fMRI study. NeuroImage. 2001; 6:1256–1267. [PubMed: 11707082]

Downar J, Crawley AP, Mikulis DJ, Davis KD. A cortical network sensitive to stimulus salience in a neutral behavioral context across multiple sensory modalities. J. Neurophysiol. 2002; 87:615–620. [PubMed: 11784775]

Folk CL, Remington RW, Johnston JC. Involuntary covert orienting is contingent on attentional control settings. J. Exp. Psychol. Hum. Percept. Perform. 1992; 18:1030–1044. [PubMed: 1431742]

Fox MD, Snyder AZ, Vincent JL, Corbetta M, Van Essen DC, Raichle ME. The human brain is intrinsically organized into dynamic, anticorrelated functional networks. Proc. Natl. Acad. Sci. U. S. A. 2005; 102:9673–9678. [PubMed: 15976020]

Fox MD, Corbetta M, Snyder AZ, Vincent JL, Raichle ME. Spontaneous neuronal activity distinguishes human dorsal and ventral attention systems. Proc. Natl. Acad. Sci. U. S. A. 2006; 103:10046–10051. [PubMed: 16788060]

Greicius MD, Krasnow B, Reiss AL, Menon V. Functional connectivity in the resting brain: a network analysis of the default mode hypothesis. Proc. Natl. Acad. Sci. U. S. A. 2003; 100:253–258. [PubMed: 12506194]

Hampson M, Driesen NR, Skudlarski P, Gore JC, Constable RT. Brain connectivity related to working memory performance. J. Neurosci. 2006; 26:13338–13343. [PubMed: 17182784]

He BJ, Snyder AZ, Vincent JL, Epstein A, Shulman GL, Corbetta M. Breakdown of functional connectivity in frontoparietal networks underlies behavioral deficits in spatial neglect. Neuron. 2007; 53:905–918. [PubMed: 17359924]

Indovina I, Macaluso E. Dissociation of stimulus relevance and saliency factors during shifts of visuospatial attention. Cereb. Cortex. 2007; 17:1701–1711. [PubMed: 17003078]

Kerr DL, Gusnard DA, Snyder AZ, Raichle ME. Effect of practice on reading performance and brain function. NeuroReport. 2004; 15:607–610. [PubMed: 15094461]

Kincade JM, Abrams RA, Astafiev SV, Shulman GL, Corbetta M. An event-related functional magnetic resonance imaging study of voluntary and stimulus-driven orienting of attention. J. Neurosci. 2005; 25:4593. [PubMed: 15872107]

Lang, PJ.; Bradley, MM.; Cuthbert, BN. Technical Report A-8. University of Florida; Gainesville, FL: 2008. International affective picture system (IAPS): Affective ratings of pictures and instruction manual.

Macaluso E, Frith CD, Driver J. Directing attention to locations and to sensory modalities: multiple levels of selective processing revealed with PET. Cereb. Cortex. 2002; 12:357–368. [PubMed: 11884351]

Marois R, Leung HC, Gore J. A stimulus-driven approach to object identity and location processing in the human brain. Neuron. 2000; 25:717–728. [PubMed: 10774738]

Mason MF, Norton MI, Van Horn JD, Wegner DM, Grafton ST, Macrae CN. Wandering minds: the default network and stimulus-independent thought. Science. 2007; 315:393–395. [PubMed: 17234951]

Mazoyer B, Zago L, Mellet E, Bricogne S, Etard O, Houdé O, Crivello F, Joliot M, Petit L, Tzourio-Mazoyer N. Cortical networks for working memory and executive functions sustain the conscious resting state in man. Brain Res. Bull. 2001; 54:287–298. [PubMed: 11287133]

McKiernan KA, Kaufman JN, Kucera-Thompson J, Binder JR. A parametric manipulation of factors affecting task-induced deactivation in functional neuroimaging. J. Cogn. Neurosci. 2003; 15:394–408. [PubMed: 12729491]

Michelon P, Snyder AZ, Buckner RL, McAvoy M, Zacks JM. Neural correlates of incongruous visual information. An event-related fMRI study. NeuroImage. 2003; 19:1612–1626. [PubMed: 12948716]

Miller EK, Cohen JD. An integrative theory of prefrontal cortex function. Annu. Rev. Neurosci. 2001; 21:167–202. [PubMed: 11283309]

Ojemann J, Akbudak E, Snyder A, McKinstry R, Raichle M, Conturo T. Anatomic localization and quantitative analysis of gradient refocused echo-planar fMRI susceptibility artifacts. NeuroImage. 1997; 6:156–167. [PubMed: 9344820]

Pessoa L, Gutierrez E, Bandettini P, Ungerleider L. Neural correlates of visual working memory: fMRI amplitude predicts task performance. Neuron. 2002; 35:975–987. [PubMed: 12372290]

Posner MI, Snyder CR, Davidson BJ. Attention and the detection of signals. J. Exp. Psychol. 1980; 109:160–174. [PubMed: 7381367]

Raichle ME, MacLeod AM, Snyder AZ, Powers WJ, Gusnard DA, Shulman GL. A default mode of brain function. Proc. Natl. Acad. Sci. U. S. A. 2001; 98:676–682. [PubMed: 11209064]

Ralchle ME, Snyder AZ. A default mode of brain function: a brief history of an evolving idea. NeuroImage. 2007; 37:1083–1090. [PubMed: 17719799]

Sabatinelli D, Bradley MM, Fitzsimmons JR, Lang PJ. Parallel amygdala and inferotemporal activation reflect emotional intensity and fear relevance. NeuroImage. 2005; 24:1265–1270. [PubMed: 15670706]

Sakai K, Rowe JB, Passingham RE. Active maintenance in prefrontal area 46 creates distractor-resistant memory. Nat. Neurosci. 2002; 5:479–484. [PubMed: 11953754]

Serences JT, Shomstein S, Leber AB, Golay X. Coordination of voluntary and stimulus-driven attentional control in human cortex. Psychol. Sci. 2005; 16:114–122. [PubMed: 15686577]

Shulman GL, Fiez JA, Corbetta M, Buckner RL, Miezin FM, Raichle ME, Perterson SE. Common blood flow changes across visual tasks: II. decreases in cerebral cortex. J. Cogn. Neurosci. 1997; 9:648–663.

Shulman GL, McAvoy MP, Cowan MC, Astafiev SV, Tansy AP, d'Avossa G, Corbetta M. Quantitative analysis of attention and detection signals during visual search. J. Neurophysiol. 2003; 90:3384–3397. [PubMed: 12917383]

Shulman GL, Astafiev SV, McAvoy MP, d'Avossa G, Corbetta M. Right TPJ deactivation during visual search: functional significance and support for a filter hypothesis. Cereb. Cortex. 2007; 17:2625–2633. [PubMed: 17264254]

Sternberg, S. The discovery of processing stages: Extensions of Donders' method. In: Koster, WG., editor. Attention and performance II. North-Holland, Amsterdam: 1969.

Talairach, J.; Tournoux, P. Co-planar stereotaxic atlas of the human brain. Thieme; New York: 1988.

Todd JJ, Fougnie D, Marois R. Visual short-term memory load suppresses temporo-parietal junction activity and induces inattentional blindness. Psychol. Sci. 2005; 16:965–972. [PubMed: 16313661]

Treue S. Visual attention: the where, what, how and why of saliency. Curr. Opin. Neurobiol. 2003; 13:428–432. [PubMed: 12965289]

Van Essen DC. A Population-Average, Landmark- and Surface-based (PALS) atlas of human cerebral cortex. NeuroImage. 2005; 28:635–662. [PubMed: 16172003]

Worsley KJ, Friston KJ. Analysis of fMRI time-series revisited—again. NeuroImage. 1995; 2:173–181. [PubMed: 9343600]

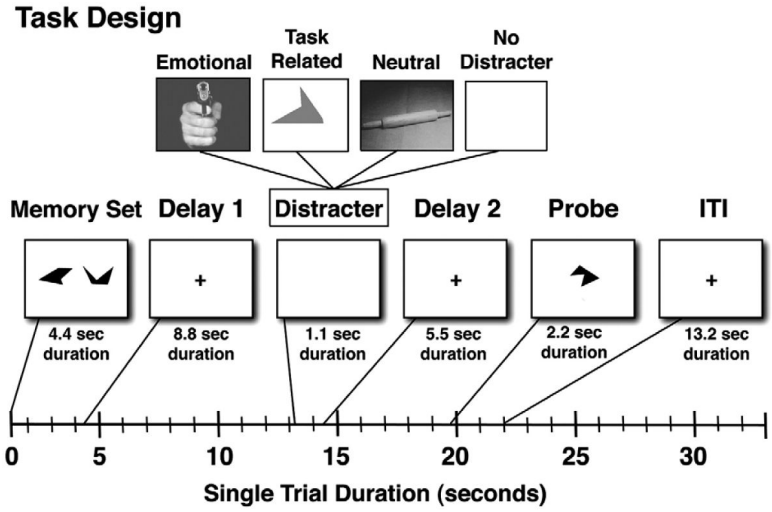

Fig. 1.

Task design. A schematic representation of a single trial is shown along with different components and their onsets marked along the timeline. Each box represents a trial component with the duration marked bellow. First, subjects were presented with a set of complex geometric shapes, which they were instructed to memorize, followed by a delay. Next, during the middle phase of the trial subjects saw either: (1) an emotional distracter; (2) a task-related geometric shape distracter of a different color distinguishing it from the probe; (3) a neutral distracter; or (4) no distraction. This was followed by another delay. Finally, subjects were shown a probe for which they indicated using a button response if it was part of the memorized set or not.

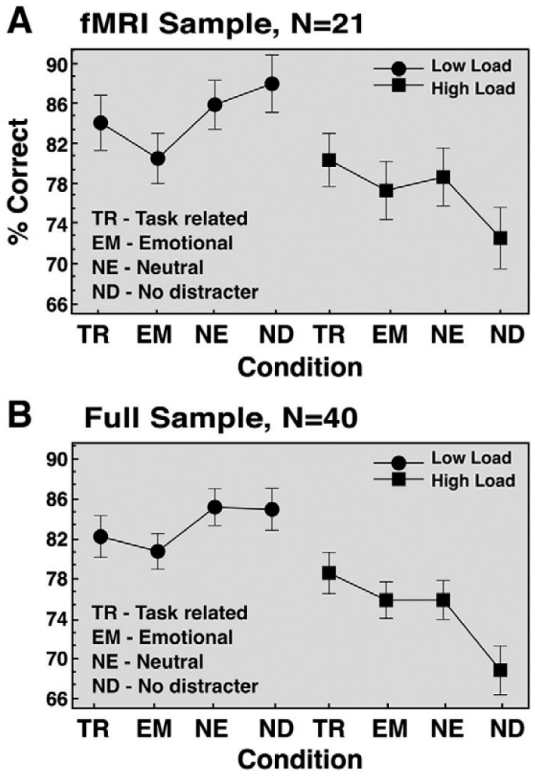

Fig. 2.

Behavioral results. Mean accuracy (expressed as % correct) is shown for task-related, emotional, neutral distracter conditions as well as distracter-free trials across two load levels (high load Behavioral results. Mean accuracy (expressed as % correct) is shown for task-related, emotional, neutral distracter conditions as well as distracter-free trials across two load levels (high load=3 shapes, low load=2 shapes). Results are shown for the (A) fMRI sample only (*N*=21); and (B) full sample comprised of fMRI and an additional out-of-scanner sample (*N*=40). Both samples received identical versions of the task. Error bars represent ±1 standard error of the mean.

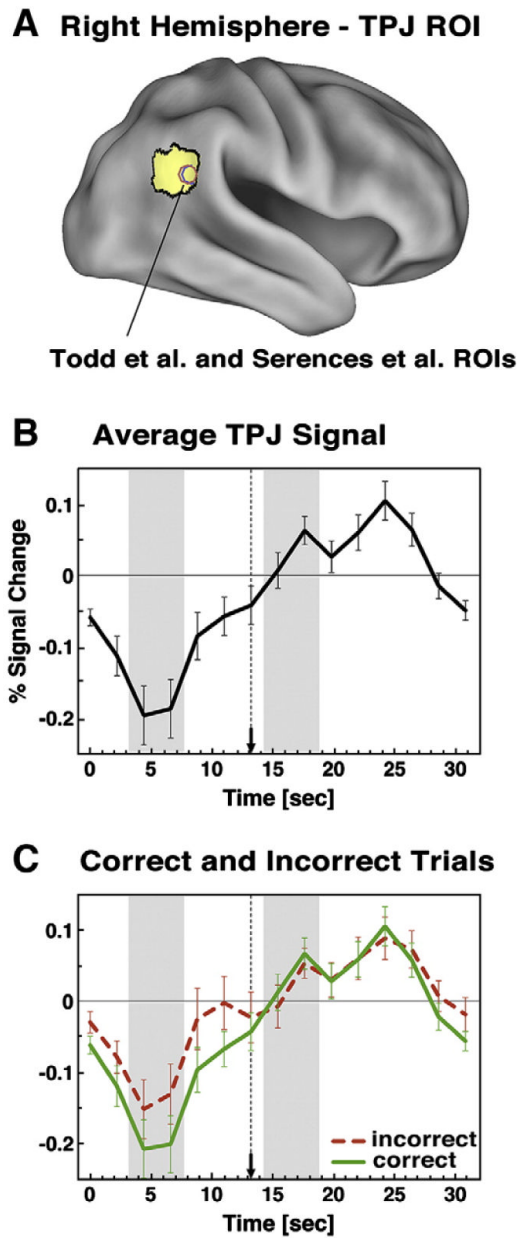

Fig. 3.

TPJ time courses. (A) TPJ ROI is shown on the right lateral surface rendering along with foci from previous studies. (B) Average event-related time course is shown for the TPJ ROI averaged across distracter types and loads, given no differences at encoding. (C) Average time course extracted from TPJ ROI is shown for correct (green) and incorrect (red-dotted) trials collapsed across loads and distracter types. Distracter onset is marked by a dotted vertical line ending in an arrow. Encoding and distracter phases are marked with grey bars. Error bars represent ±1 standard error of the mean.

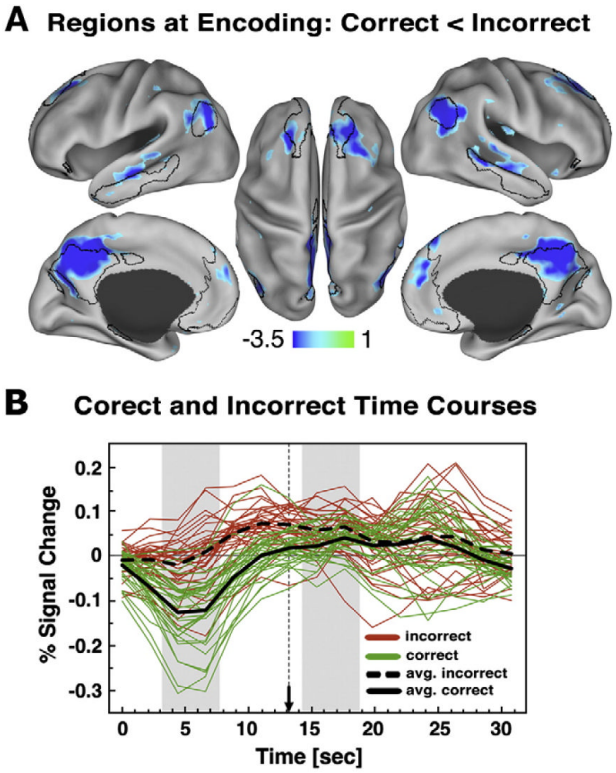

Fig. 4.

Other regions showing less signal for correct than incorrect trials during encoding. (A) Regions showing less signal for correct than incorrect trials during the encoding phase closely match the Fox and colleagues (2005) default network regions, which are shown using black border outlines. Here, we show the foci using a $Z>2.5$ threshold demonstrating that even with a lower cutoff the deactivations are centered mainly around the default network regions and not elsewhere. (B) Average event-related time courses are shown for correct (green) and incorrect (red) trials across all the peak ROIs identified from the map in the top panel after it was corrected for multiple comparisons using cluster size algorithms to ensure whole-brain false positive rates of $p<0.05$. Each line represents signal for a single ROI averaged across all trial types given no differences between them during encoding. The black lines show the average response across all peak ROIs for correct (solid) and incorrect (dotted) trials. Distracter onset is marked by a dotted vertical line ending in an arrow. Encoding and distracter phases are marked with grey bars.

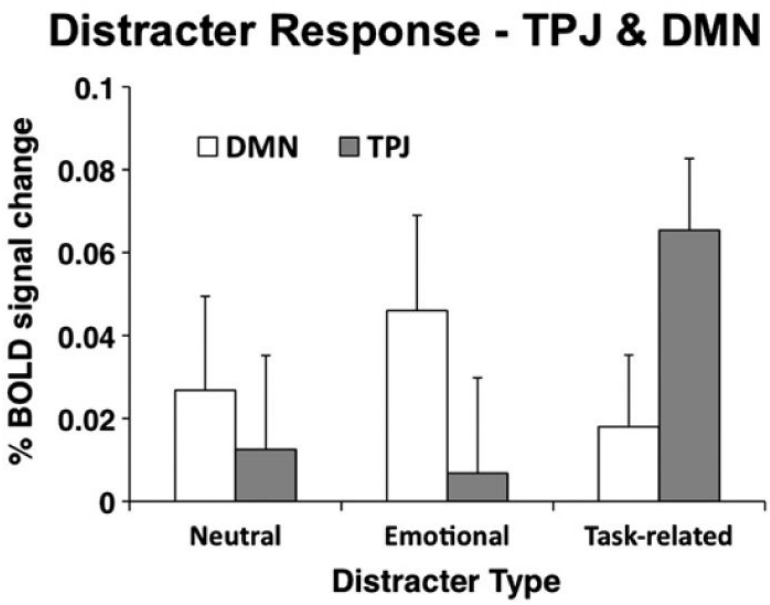

Fig. 5.

TPJ and default network distracter response. Magnitudes associated with the distracter response component obtained using the assumed GLM are shown for the TPJ (gray bars) and default network (DMN) (white bars) across different distracter types. Magnitudes are collapsed across loads given no differences as a function of load. Error bars represent ± 1 standard error of the mean.

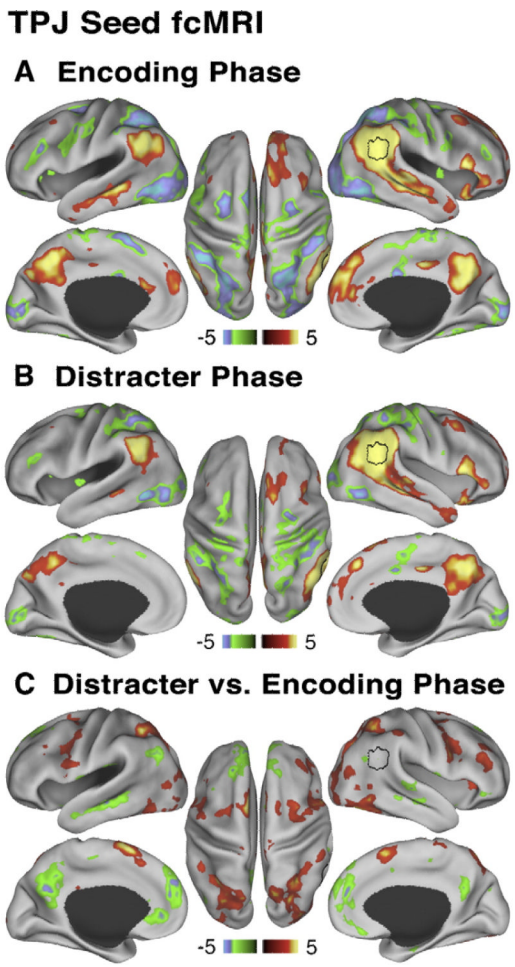

Fig. 6.

Relationship between TPJ and default network at encoding and distracter phases. All maps are shown using Z statistics. (A) During the encoding phase TPJ seed ROI shows positive correlations (red-yellow colors) with main nodes of the default network and negative correlations (green-blue colors) with main components of the dorsal task network. (B) During the distracter phase the pattern is similar, but attenuated. (C) Maps show results of a paired *t*-test comparing TPJ ROI trial-based connectivity during distracter vs. encoding phase. Red-yellow map shows regions where correlations with the TPJ seed increased from encoding to distracter phase, whereas the green-blue map shows regions where correlations with the TPJ seed decreased from encoding to distracter phase, indicative of “de-coupling”. We show the map at $Z>2.5$ to illustrate that the TPJ (shown in black border outline) “de-couples” mainly from the default network and not other cortical regions, but `couples' more strongly with the dorsal task network. All peaks shown were present after applying a multiple comparison correction using cluster size algorithms to ensure whole-brain false positive rates of $p<0.05$.

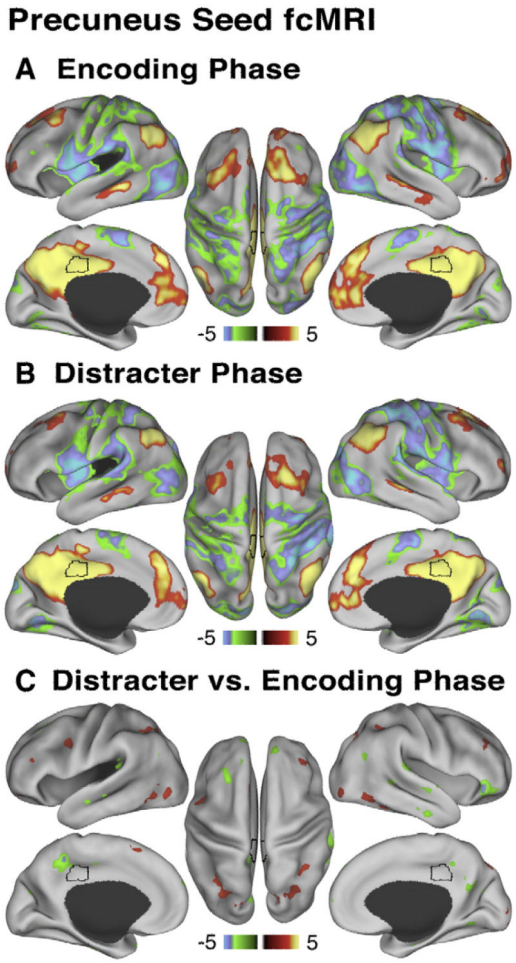

Fig. 7.

Relationship between precuneus and default network at encoding and distracter phases. All maps are shown using *Z* statistics. Here we used an independent precuneus seed to demonstrate that: (A) During the encoding phase precuneus shows positive correlations (red-yellow colors) with the rest of the default network and negative correlations (green-blue colors) with the dorsal task network, analogous to the TPJ connectivity map at encoding. (B) During the distracter phase the pattern is largely similar. (C) Maps show results of a paired *t*-test comparing precuneus seed trial-based connectivity during distracter vs. encoding phase. Red-yellow maps shows regions where correlations with the precuneus seed increased from encoding to distracter phase, whereas the green-blue map shows regions where correlations with the precuneus seed decreased from encoding to distracter phase. As before, we show the map at $Z>2.5$ threshold to indicate that, in contrast to TPJ, a canonical default system node does not show such "de-coupling," also illustrated quantitatively for the entire DMN in Fig. 8.

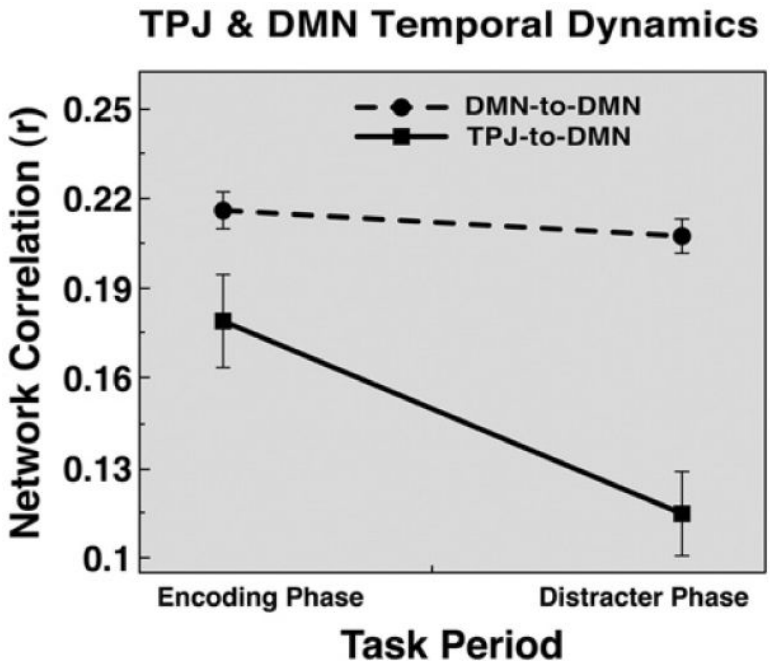

Fig. 8.

TPJ and default network functional connectivity temporal dynamics. Seed-based pairwise correlations are shown averaged across all TPJ-to-DMN correlations (i.e. TPJ and each DMN node, solid line with squares) and all DMN-to-DMN correlations (i.e. each DMN node with every other DMN node, dotted line with circles). The correlations are shown at encoding and distracter phases. Overall, DMN-to-DMN connections remain stable across the WM phases, while TPJ-to-DMN functional connectivity "weakens" from encoding to distracter phase. Error bars represent ± 1 standard error of the mean.